JACS
JOURNAL OF THE AMERICAN CHEMICAL SOCIETY
Article
pubs.acs.org/JACS

Tuning the Potentials of "Extra" Electrons in Colloidal *n*-Type ZnO Nanocrystals via Mg^{2+} Substitution

Alicia W. Cohn, Kevin R. Kittilstved,† and Daniel R. Gamelin*

Department of Chemistry, University of Washington, Seattle, Washington 98195-1700, United States

ABSTRACT: Colloidal reduced ZnO nanocrystals are potent reductants for one-electron or multielectron redox chemistry, with reduction potentials tunable via the quantum confinement effect. Other methods for tuning the redox potentials of these unusual reagents are desired. Here, we describe synthesis and characterization of a series of colloidal $Zn_{1-x}Mg_xO$ and $Zn_{0.98-x}Mg_xMn_{0.02}O$ nanocrystals in which Mg^{2+} substitution is used to tune the nanocrystal reduction potential. The effect of Mg^{2+} doping on the band-edge potentials of ZnO was investigated using electronic absorption, photoluminescence, and magnetic circular dichroism spectroscopies. Mg^{2+} incorporation widens the ZnO gap by raising the conduction-band potential and lowering the valence-band potential at a ratio of 0.68:0.32. Mg^{2+} substitution is far more effective than Zn^{2+} removal in raising the conduction-band potential and allows better reductants to be prepared from $Zn_{1-x}Mg_xO$ nanocrystals than can be achieved via quantum confinement of ZnO nanocrystals. The increased conduction-band potentials of $Zn_{1-x}Mg_xO$ nanocrystals compared to ZnO nanocrystals are confirmed by demonstration of spontaneous electron transfer from *n*-type $Zn_{1-x}Mg_xO$ nanocrystals to smaller (more strongly quantum confined) ZnO nanocrystals.

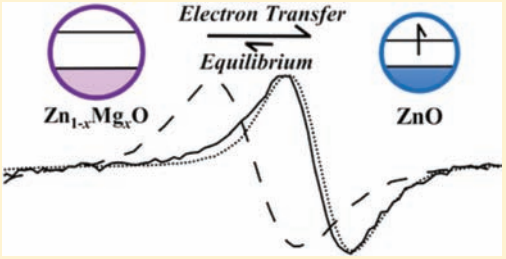

INTRODUCTION

Colloidal ZnO nanocrystals can be "charged" photochemically to give kinetically stable suspensions of powerful reductants.[1−7] The extra conduction-band electrons added by this process can be monitored by electronic absorption[1−4] or electron paramagnetic resonance (EPR) spectroscopies.[3−6] When exposed to air or mixed with suitable electron acceptors (e.g., uncharged nanocrystals or molecules), these reduced nanocrystals are rapidly reoxidized,[1−4,7−9] making charged ZnO nanocrystals attractive reagents for fundamental studies of interfacial electron-transfer processes involving semiconductor nanostructures. The conduction band-edge potentials of colloidal ZnO nanocrystals can be tuned via quantum confinement to achieve a total range of ∼150 mV, and multiple electrons can be introduced into a single nanocrystal,[4,9−12] making them unusually versatile reductants for one-electron or multielectron redox chemistries.[13] For some reactions, even stronger reductants may be desired than can be achieved via quantum confinement. Here, we examine the use of Mg^{2+} substitution to tune ZnO nanocrystal reduction potentials. Isovalent cation substitution is known to alter the conduction-band potentials of many semiconductor nanocrystals[14−17] and hence should provide an effective means of tuning the chemical reactivities of these unusual colloidal ZnO-based reagents, but this parameter has not yet been thoroughly examined.

Interest in $Zn_{1-x}Mg_xO$ frequently stems from its potential applications in optoelectronic devices, for example as a barrier layer in ZnO-based heterostructures,[16−19] in UV sensors,[20] and in ZnO-based lasing devices.[21] $Zn_{1-x}Mg_xO$ thin films have been prepared by a variety of techniques including pulsed laser deposition (PLD),[22] low-temperature chemical vapor deposition,[23] molecular beam epitaxy,[24] radio frequency magnetron sputtering,[25] and sol−gel deposition.[26] Colloidal $Zn_{1-x}Mg_xO$ nanocrystals have been synthesized by high-temperature, air-free methods.[27,28] Mg^{2+} and Zn^{2+} have similar tetrahedral ionic radii (0.57 and 0.60 Å),[29] contributing to the relatively high solid solubility of Mg^{2+} in wurtzite ZnO. In epitaxial thin films made by PLD, for example, Mg^{2+} is incorporated into the wurtzite lattice structure up to $x \approx 0.33$ without detectable phase segregation.[22] Previous studies of $Zn_{1-x}Mg_xO$ thin films and nanocrystals have primarily focused on characterizing the change in band gap with x using electronic absorption and luminescence spectroscopies.[22,25,28,30,31] For many applications, however, the specific band offsets at $Zn_{1-x}Mg_xO$/ZnO interfaces are important,[16,17,24] but quantification of the shifts of individual bands with x is more challenging than quantification of the change in the energy gap.

We report here the synthesis of a series of colloidal wurtzite $Zn_{1-x}Mg_xO$ and $Zn_{1-x-y}Mg_xMn_yO$ nanocrystals using a simple room-temperature procedure developed previously for doping ZnO nanocrystals with Co^{2+}, Ni^{2+}, or Mn^{2+} ions.[32,33] We demonstrate that shifts of the individual band-edge potentials with x can be determined by measurement of trap photoluminescence energies, Mn^{2+} donor-type photoionization energies, and band-to-band transition energies. These data indicate that increasing x in these wurtzite $Zn_{1-x}Mg_xO$ nanocrystals increases the energy gap primarily by raising the conduction-band potential, but also by shifting the valence-band potential. Mg^{2+} substitution is found to be much more effective than quantum confinement in raising the conduction-band potentials of ZnO-based nanocrystals. The absolute

Received: February 28, 2012
Published: April 19, 2012

   dx.doi.org/10.1021/ja3019934 | *J. Am. Chem. Soc.* 2012, 134, 7937−7943

increase in conduction-band potential with Mg^{2+} incorporation is unambiguously confirmed by demonstration of spontaneous inter-nanocrystal electron transfer from $Zn_{1-x}Mg_xO$ nanocrystals to more strongly quantum-confined ZnO nanocrystals.

EXPERIMENTAL SECTION

Synthesis. Colloidal ZnO and $Zn_{1-x-y}Mg_xMn_yO$ nanocrystals were synthesized using a base-initiated hydrolysis/condensation procedure described previously.[32,33] Briefly, 1.6 equiv of 0.5 M tetramethylammonium hydroxide in ethanol was added dropwise to a 0.1 M solution of zinc acetate (+manganese acetate as desired) in dimethylsulfoxide (DMSO). For $Zn_{1-x}Mg_xO$ nanocrystals, magnesium acetate was added to the DMSO solution along with the zinc acetate while keeping the cation-to-hydroxide ratio constant. To obtain nanocrystals of different diameters from a given synthesis, aliquots were removed from the growth solution at four different stages: immediately following the addition of the base, 30 min later, 2 h later, and 1−3 days later. Between 2 h and 3 days, the growth solution was heated at 50 °C. For each aliquot, the nanoparticles were washed by precipitating with heptane and resuspending in ethanol. Mg^{2+} addition inhibits nanocrystal growth, and to achieve the largest nanocrystals with high Mg^{2+} content, the nanocrystals were heated in neat dodecylamine at 160 °C for ∼20 min before washing. The experiments here were performed on dodecylamine-ligated nanocrystals suspended in toluene, prepared by adding dodecylamine to an ethanolic suspension of nanocrystals until the nanocrystals precipitated (at ∼200−700:1 mol ratio), followed by centrifugation and resuspension in toluene.

Physical Measurements. Electronic absorption spectra were collected at room temperature using a Cary 500 spectrometer. Photoluminescence spectra were collected at room temperature by exciting the colloidal nanocrystals with either 337 nm light from a nitrogen laser or 330 nm light from a 200 W tungsten−halogen lamp dispersed through a 0.3 m monochromator, detecting with a nitrogen-cooled CCD. Magnetic circular dichroism (MCD) spectra were collected using an Aviv 40DS spectropolarimeter with a water-cooled electromagnet. Mg^{2+} and Mn^{2+} concentrations ($x \pm 0.01$) were determined analytically using inductively coupled plasma mass spectrometry and atomic emission spectroscopy (ICP-MS and ICP-AES). In some cases, data are reported using nominal Mg^{2+} concentrations (x_n) rather than analytical concentrations (x), where x_n is the Mg^{2+} cation mole fraction of the initial reaction mixture. The two values are within 10% of one another in all cases where x was determined (with the remaining cations removed by washing), making this representation acceptable for relative measurements. EPR spectra were collected using a Bruker Elexys E580 X-band spectrometer. EPR spectra were recorded under steady-state conditions achieved by continuously irradiating samples (with a Hg/Xe arc-lamp) open to air within the EPR cavity. These EPR signals decay in the dark with time constants of $\tau \approx 1$ min, i.e., sufficiently slow for inter-nanocrystal electron transfer ($\tau < 5$ μs) to reach equilibrium when mixtures of nanocrystals are used. In all cases, essentially indistinguishable EPR results have been obtained under anaerobic conditions without continuous irradiation. EPR g values were measured using using diphenylpicrylhydrazyl (DPPH) as an internal reference. X-ray diffraction (XRD) data were collected using a Bruker F8 Focus instrument with a Cu Kα radiation source operating at 40 kV and 40 mA, with KCl as an internal reference.

Band gap energies (E_g) were approximated by the energies at which the optical density at the absorption edge reached half of its maximum value. Diameters of $Zn_{1-x}Mg_xO$ and $Zn_{1-x-y}Mg_xMn_yO$ nanocrystals were estimated from XRD data using the Scherrer equation.[34] Diameters of ZnO nanocrystals were estimated from electronic absorption spectra using empirical relationships.[35,36]

RESULTS AND ANALYSIS

Nanocrystal Characterization. Figure 1a shows powder XRD data collected for $d = 4.3$ nm $Zn_{1-x}Mg_xO$ nanocrystals at $x = 0$ and 0.18, with x determined analytically (see Experimental Section). The peaks between 30° and 38° are characteristic of the wurtzite lattice structure, and their broad peak widths confirm formation of nanocrystals, as seen previously with this synthetic method.[32,33,37] The sharp peak at 40.5° is from KCl that was added as an internal reference. Note the absence of any detectable rocksalt MgO peak at 42.5°. There are conflicting results in the literature concerning the direction of the changes in a and c lattice parameters with increasing Mg^{2+} incorporation,[22,31] but in all cases these changes are small. In our samples, a also does not shift significantly over the range $0 \le x \le 0.18$, but very small shifts would be obscured by the broad peak widths of these nanocrystals. Figure 1b shows transmission electron microscopy (TEM) images of $Zn_{1-x}Mg_xO$ nanocrystals at $x_n = 0.20$, confirming their quasi-spherical shapes and crystallinity. Overall, these data are consistent with formation of $Zn_{1-x}Mg_xO$ nanocrystals.

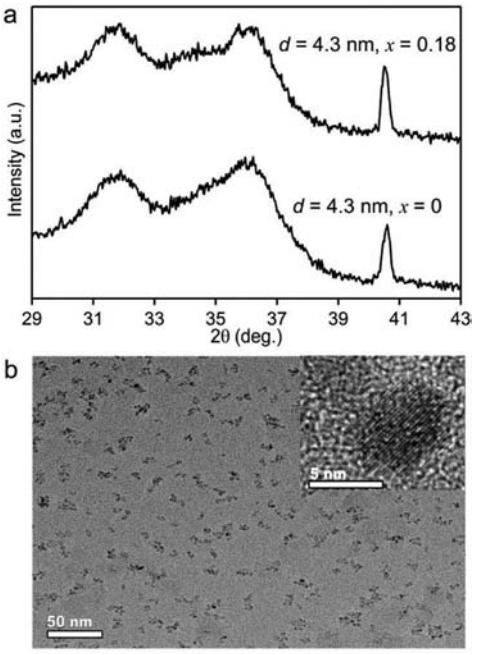

Figure 1. (a) Powder XRD data collected for $d = 4.3$ nm $Zn_{1-x}Mg_xO$ nanocrystals with $x = 0$ and $x = 0.18$. The Mg^{2+} contents (x) were determined analytically, with an estimated uncertainty of ±0.01. The peak at $2\theta = 40.5°$ comes from KCl, which was included as an internal reference. (b) TEM images of $Zn_{1-x}Mg_xO$ nanocrystals ($x_n = 0.20$).

Spectroscopic Properties. Figure 2a plots electronic absorption and photoluminescence spectra collected for a series of $Zn_{1-x}Mg_xO$ nanocrystals with $d >$ ∼6.0 nm (where quantum confinement effects are minimal) and with different values of x. The absorption edge shifts to higher energy with increasing x, as summarized in Figure 2b. The photoluminescence spectra are dominated by midgap trap luminescence centered at ∼2.2 eV. This trap luminescence also shifts to higher energy with increasing x, as summarized in Figure 2b.

A linear fit of the absorption data yields $E_g = (3.41 + 1.04x)$ eV. A linear fit of the PL data yields $E_{PL} = (2.09 + 0.67x)$ eV. The absorption and PL features thus both shift to higher energy with increasing x, but with different slopes. The dependence of E_g on x is only half as large as some that have been reported in the literature for bulk and nanocrystalline $Zn_{1-x}Mg_xO$ (∼$2x$ eV),[22,25,27,38] but is approximately three times larger than

dx.doi.org/10.1021/ja3019934 | J. Am. Chem. Soc. 2012, 134, 7937−7943

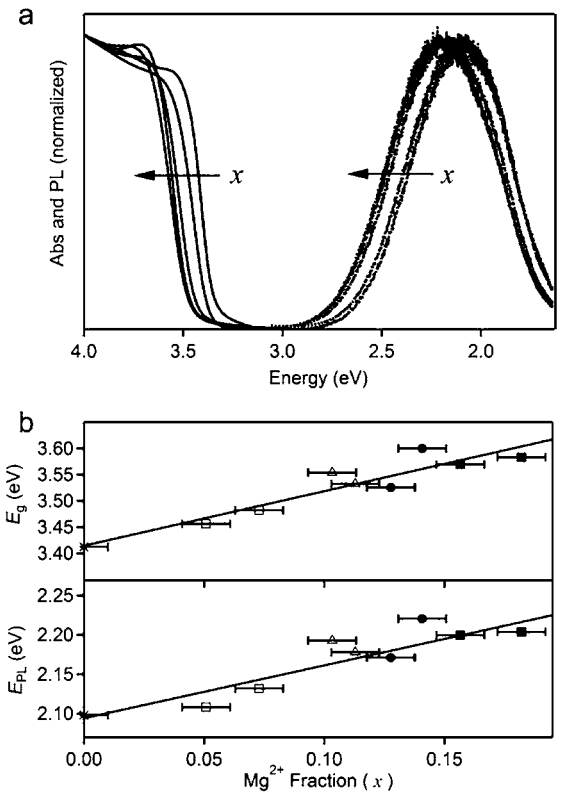

Figure 2. (a) Room-temperature electronic absorption (solid line) and luminescence (dotted line) spectra of colloidal $Zn_{1-x}Mg_xO$ ($0 \le x \le 0.18$) nanocrystals with diameters $d > 6.0$ nm, where quantum confinement is negligible. The arrows indicate direction of increasing x. (b) Band-gap energies (half-maxima of electronic absorption spectra) for ZnO and $Zn_{1-x}Mg_xO$ nanocrystals with $d > 5.0$ nm and trap emission energies for the same samples plotted vs x. To illustrate agreement between x and x_n, the data are marked using symbols corresponding to $x_n = 0$ (star), 0.05 (open square), 0.10 (open triangle), 0.15 (closed circle), and 0.20 (closed square). The best-fit lines are described by $E_g = (3.41 + 1.04x)$ eV and $E_{PL} = (2.09 + 0.67x)$ eV.

others.[31] We tentatively attribute these discrepancies to inhomogeneous Mg^{2+} distributions, for example possible Mg^{2+} enrichment at the nanocrystal surfaces in our case. Importantly, these discrepancies illustrate the need for a method of assessing band potentials that is *independent* of detailed knowledge of the Mg^{2+} distribution. As shown below, photoluminescence and EPR spectroscopies are both effective in this capacity.

The visible trap luminescence of colloidal ZnO nanocrystals has been attributed to recombination of an electron in or near the conduction band with a deeply trapped hole.[39−43] Despite many years of investigation, the microscopic identities of the active traps remain poorly understood. Because of the large surface-to-volume ratios, the surface chemistry strongly influences the luminescence of ZnO nanocrystals.[8,37,42,44−47] For example, in nanocrystals prepared by this and other synthetic methods, correlations have been observed between the presence of surface hydroxide moieties and visible trap luminescence intensity,[37,45] suggesting surface hole localization in this excited state. Similarly, surface modification with small cationic or anionic moieties strongly alters this trap PL.[47] Although the microscopic identities of the active traps remain unclear, the holes involved in this PL are deeply trapped and consequently insensitive to quantum confinement. The slope of a plot of E_{PL} vs E_g for a series of quantum confined ZnO nanocrystals thus simply reflects the dependence of the conduction band potential on electron quantum confinement.[41] Experimentally, this slope was found to be ∼0.60 for ZnO nanocrystals,[41] in good agreement with expectations from the effective mass approximation (∼0.64).

A similar analysis can now be applied to understanding the visible trap PL of $Zn_{1-x}Mg_xO$ nanocrystals. Figure 3 replots the

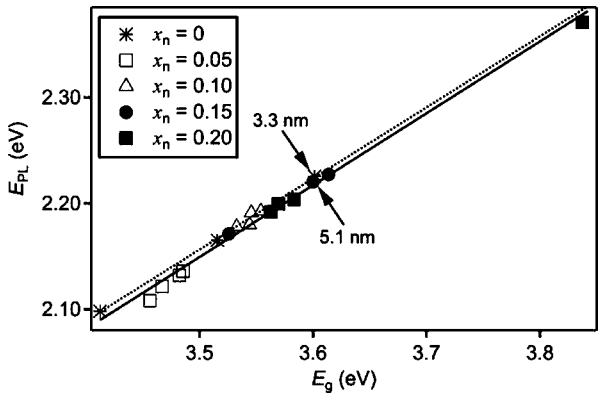

Figure 3. Peak energy of the visible trap luminescence plotted versus the band gap energy (half-maxima of the electronic absorption spectra) for ZnO and $Zn_{1-x}Mg_xO$ nanocrystals of different diameters and values of x. A linear fit of the $Zn_{1-x}Mg_xO$ data yields a slope of 0.68 (solid). A linear fit of the ZnO data (*) yields a slope of 0.67 (dotted). The arrows highlight the fact that a $d = 3.3$ nm ZnO (*) nanocrystal and a $d = 5.1$ nm $Zn_{0.85}Mg_{0.15}O$ (●) nanocrystal have the same spectroscopic properties.

data from Figure 2 (along with data from samples where x was not determined analytically) as E_{PL} vs E_g. This representation allows shifts in the conduction band potentials to be assessed without explicit consideration of x and without any assumption about Mg^{2+} spatial distribution. Plotting the data in this way yields a straight line with slope $\Delta E_{PL}/\Delta E_g = 0.68$. The slope obtained here for ZnO nanocrystals due solely to quantum confinement is 0.67, in good agreement with previous observations.[41] If Mg^{2+} substitution only changed the conduction band potential as suggested by DOS calculations,[48,49] then $\Delta E_{PL}/\Delta E_g \approx 1$. Instead, the slope of 0.68 in Figure 3 implies that Mg^{2+} incorporation into ZnO shifts *both* the conduction- and valence-band potentials in a ratio ΔE_{CB}:$\Delta E_{VB} \approx 0.68$:0.32. Whereas the shift in CB potential reflects the absence of resonance between Mg^{2+} and Zn^{2+} 4s orbitals, the shift in VB potential is likely due to the impact of the different Mg^{2+} and Zn^{2+} electronegativities on M^{2+}−O^{2-} bonding. Previous valence-band XPS measurements and modeling studies of ZnO quantum wells with $Zn_{1-x}Mg_xO$ barrier layers have estimated ratios of ΔE_{CB}:ΔE_{VB} between 1:1 and 0.7:0.3,[16,17,24] in good agreement with the ratio found here for the colloidal $Zn_{1-x}Mg_xO$ nanocrystals.

It is conceivable that the nature of the luminescent trap state is not independent of Mg^{2+} as assumed in the analysis above. As an independent crosscheck of the impact of Mg^{2+} incorporation on the conduction-band potential, $Zn_{1-x}Mg_xO$ nanocrystals were therefore prepared with Mn^{2+} as a co-dopant. Mn^{2+} in ZnO possesses a midgap donor-type photoionization state formally involving a $Mn^{2+} \rightarrow$ conduction band charge transfer ($ML_{CB}CT$) excitation,[15,50,51] although some researchers favor a

dx.doi.org/10.1021/ja3019934 | J. Am. Chem. Soc. 2012, 134, 7937−7943

Zhang–Rice-like description of these excited states.[52,53] This $ML_{CB}CT$ transition appears as a broad structureless midgap band in electronic absorption spectra and as a derivative feature in MCD spectra of Mn^{2+}-doped ZnO.[15,33,54]

Figure 4 shows the 298 K electronic absorption and 298 K, 1 T MCD spectra of a series of colloidal $Zn_{0.98-x}Mg_xMn_{0.02}O$

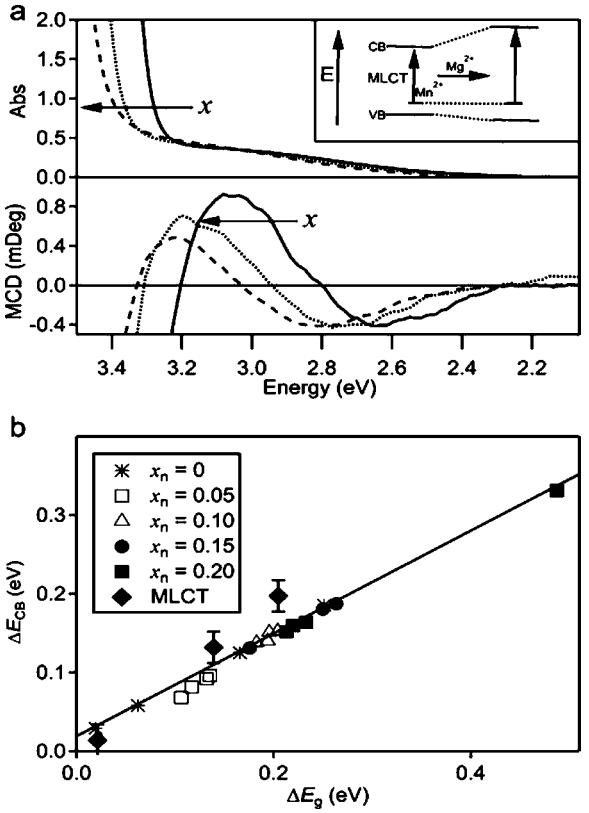

Figure 4. (a) 298 K electronic absorption and 298 K, 1 T MCD spectra of $Zn_{0.98-x}Mg_xMn_{0.02}O$ (x = 0, 0.05, 0.10 (±0.01)) colloidal nanocrystals, with diameters of 8.0, 5.0, and 4.6 nm (±0.5 nm), respectively, as determined by XRD analysis. The arrows indicate the direction of increasing x. Optical densities of the $ML_{CB}CT$ transition were below 0.60 for the MCD measurements. The y axes correspond to those of the x = 0 measurement. (b) Plot of ΔE_{CB} vs ΔE_g from the MCD data (diamonds) and from the PL data of Figure 3. The inset to (a) describes the $ML_{CB}CT$ shift with x schematically.

nanocrystals with x = 0.00, 0.05, and 0.10. The $ML_{CB}CT$ transition is observed in the absorption spectra of all three samples as a broad band centered at ~3.0 eV, and as a derivative-shaped MCD feature over the same energies. The data show a clear shift of this $ML_{CB}CT$ transition to higher energy with increasing x, with $\Delta E_{CT} \approx 190$ meV at x = 0.10. Because Mn^{2+} is a deep donor in ZnO, its potential is pinned,[55–57] and this shift in the $ML_{CB}CT$ transition energy is predominantly attributable to the change in conduction band potential, ΔE_{CB}. All three samples are close to the bulk size regime, and quantum confinement cannot account for more than ~10 meV of the observed shift. Plotting the data from Figure 4 as ΔE_{CB} vs ΔE_g allows direct comparison with the data from Figure 3, and the results from the two experiments agree well. These data thus provide an independent demonstration that Mg^{2+} substitution raises the CB potential of the ZnO nanocrystals.

Charged $Zn_{1-x}Mg_xO$ Nanocrystals. The motivation for preparing colloidal $Zn_{1-x}Mg_xO$ nanocrystals was to explore Mg^{2+} substitution as an approach to tuning ZnO nanocrystal reduction potentials relevant to actual electron-transfer reactions. To evaluate the properties of the CB electrons directly, these nanocrystals were reduced photochemically to form colloidal n-type $Zn_{1-x}Mg_xO$ nanocrystals.[1–7] As demonstrated previously, EPR spectroscopy is a superb tool for probing the properties of the extra electrons in colloidal n-type ZnO nanocrystals[3–7] and in ZnO nanocrystalline powders.[58–60] This technique has demonstrated that these electrons are indeed conduction-band-like, and in particular are delocalized over the entire colloidal nanocrystal volume.[5,6,61] The EPR signals of a series of n-type $Zn_{1-x}Mg_xO$ nanocrystals of different x and the same diameter are shown in Figure 5a. Figure 5b

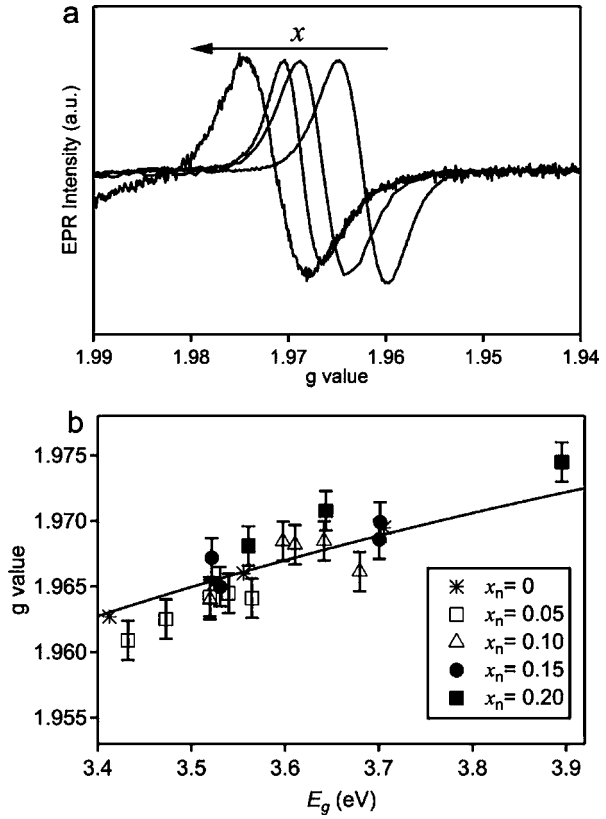

Figure 5. (a) Room-temperature EPR spectra of colloidal n-type $Zn_{1-x}Mg_xO$ (x = 0.05, 0.10, 0.13, and 0.17) nanocrystals with d > 6 nm. The arrow indicates direction of increasing x. (b) A plot of the EPR g values vs E_g for nanocrystals of different diameters and values of x_n. The solid line shows the best fit of the n-type ZnO nanocrystal data, obtained using eq 1 with P^2 = 20 eV and Δ_{SO} fitted to 35 meV.

plots these g values vs E_g (determined by electronic absorption spectroscopy), along with data collected for nanocrystals of the same x but different diameters. For a given diameter, the electron g value increases with increasing x, ranging from 1.961 to 1.975 in a similar way as can be achieved through quantum confinement alone,[5] but spanning a broader range. A similar increase in electron g values with x has been observed recently in oriented epitaxial thin films of $Zn_{1-x}Mg_xO$ grown by MBE.[62]

From Figure 5, Mg^{2+} substitution and quantum confinement yield indistinguishable relationships between g and E_g, in excellent agreement with the results shown in Figure 3. A **k·p** perturbation model has been applied successfully to describe

dx.doi.org/10.1021/ja3019934 | J. Am. Chem. Soc. 2012, 134, 7937–7943

the trend in colloidal ZnO nanocrystal g values with quantum confinement (eq 1),[5] and as shown below this model applies well to colloidal $Zn_{1-x}Mg_xO$ nanocrystals, too.

$$g^* = g_e - \frac{2}{3}\left(\frac{P^2\Delta_{SO}}{E_g(E_g + \Delta_{SO})}\right) \quad (1)$$

In eq 1, g_e is the free electron g value (2.0023), E_g is the band gap energy, P^2 is the interband mixing coefficient, and Δ_{SO} describes the valence-band spin−orbit splitting. The solid line in Figure 5b plots the curve predicted by eq 1 using P^2 = 20 eV and a best-fit value of Δ_{SO} = 35 meV, which agrees with the value of Δ_{SO} = 40 meV determined for colloidal ZnO nanocrystals in ref 5. These results indicate that the extra electrons remain CB-like in $Zn_{1-x}Mg_xO$ nanocrystals, with Mg^{2+} incorporation playing a role very similar to reduction of the electron's confinement volume. Interestingly, comparison of nanocrystals achieving the same g value via quantum confinement and via Mg^{2+} substitution reveals that Mg^{2+} incorporation is far more effective than Zn^{2+} removal in widening the energy gap, and hence in shifting the conduction-band potential and altering the g value of a conduction-band electron. For example, both d = 3.7 nm ZnO and d = 6.0 nm $Zn_{0.90}Mg_{0.10}O$ nanocrystals have g values of ∼1.965, but the former has only ∼1100 Zn^{2+} cations, whereas the latter has ∼4270 Zn^{2+} and ∼470 Mg^{2+} cations. This result highlights the efficacy of Mg^{2+} substitution in tuning the ZnO energy gap. Because Mg^{2+} is likely segregated toward the nanocrystal surfaces here, these results represent a lower limit for the tunability of nanocrystal potentials achievable using Mg^{2+} substitution.

Electron-Transfer Reactivity. The above data all suggest that Mg^{2+} substitution into ZnO nanocrystals is effective in raising the nanocrystal conduction band, which should make n-type $Zn_{1-x}Mg_xO$ nanocrystals more potent reductants than comparable n-type ZnO nanocrystals. We have previously demonstrated rapid (<5 μs) spontaneous electron transfer between colloidal ZnO quantum dots, with driving forces derived from electron quantum confinement.[7] Here, we show that such electron transfer can be used to determine the relative conduction band potentials of ZnO and $Zn_{1-x}Mg_xO$ nanocrystals under equilibrium conditions.

Figure 6 plots the EPR spectrum collected during UV irradiation of an equimolar mixture of 2.9 nm ZnO (g = 1.9695, E_g = 3.71 eV) and ∼4.0 nm $Zn_{0.75}Mg_{0.25}O$ (g = 1.9745, E_g = 3.89 eV) nanocrystals, conditions under which both nanocrystals are excited simultaneously at approximately the same rate. Because inter-nanocrystal electron transfer is fast (τ < 5 μs)[7] relative to reoxidation ($\tau \approx$ 1 min), photochemical reduction is followed by rapid equilibration of the electron population according to the relative conduction band potentials of the ZnO and $Zn_{0.75}Mg_{0.25}O$ nanocrystals. The EPR spectrum of the mixture in Figure 6 thus reports on the equilibrium distribution of electrons among ZnO and $Zn_{0.75}Mg_{0.25}O$ nanocrystals. The EPR spectra of the individual nanocrystals (charged) are also plotted in Figure 6 for comparison. Only the ZnO nanocrystals are observed in the EPR spectrum of the mixture, indicating that the electrons reside predominantly in the ZnO nanocrystals at equilibrium. This result demonstrates that $Zn_{0.75}Mg_{0.25}O$ nanocrystals are better reductants than even smaller ZnO nanocrystals, despite the greater quantum confinement in the latter. This finding agrees well with the difference in the trap luminescence energies of these two samples, from which a driving force of ∼130 mV is deduced for electron transfer from

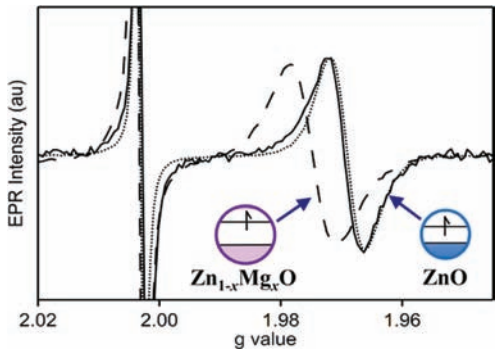

Figure 6. Room temperature EPR spectra of ZnO nanocrystals ($d \approx$ 2.9 nm, dotted), $Zn_{0.75}Mg_{0.25}O$ nanocrystals ($d \approx$ 4.0 nm, dashed), and an equimolar mixture of the two (solid), all with UV irradiation to introduce additional conduction-band electrons. The signal at g = 2.0036 is from DPPH. The observation of just ZnO electrons in the mixture spectrum indicates that the equilibrium distribution of electrons in this mixture strongly favors population of the ZnO subset of nanocrystals, confirming that the $Zn_{0.75}Mg_{0.25}O$ nanocrystals have more negative conduction band potentials.

the $Zn_{0.75}Mg_{0.25}O$ nanocrystals to the ZnO nanocrystals of Figure 6. The visible trap luminescence of ZnO-based nanocrystals can thus be used as a probe of the conduction-band reduction potentials of ZnO and related nanocrystals. Overall, the $Zn_{1-x}Mg_xO$ trap luminescence ranges from ∼2.1 to ∼2.4 eV (Figure 3), corresponding to a ∼300 mV range of tunability in nanocrystal reduction potentials. Importantly, this tunability is approximately twice as large as could be achieved from quantum confinement of ZnO nanocrystals alone (i.e., without Mg^{2+} incorporation), validating the original hypothesis that Mg^{2+} substitution is effective in this capacity.

CONCLUSION

Colloidal $Zn_{1-x}Mg_xO$ nanocrystals were synthesized by a hydrolysis and condensation reaction performed at room temperature under aerobic conditions. Mg^{2+} incorporation widens the band gap of the ZnO colloids much more than quantum confinement does by removal of the equivalent number of Zn^{2+} cations. In all other regards, Mg^{2+} substitution appears to have very similar effects as quantum confinement on the physical properties of these nanocrystals. Analysis of the trap luminescence of $Zn_{1-x}Mg_xO$ nanocrystals and the midgap $ML_{CB}CT$ transitions of $Zn_{0.98-x}Mg_xMn_{0.02}O$ nanocrystals shows that band gap widening with x involves increasing the conduction band potential and lowering the valence-band potential in a ratio of ΔE_{CB}:ΔE_{VB} = 0.68:0.32. Photochemical "charging" yields colloidal n-type $Zn_{1-x}Mg_xO$ nanocrystals, whose EPR g values agree well with those of colloidal n-type ZnO nanocrystals having the same energy gap. Charging mixtures of ZnO and $Zn_{1-x}Mg_xO$ nanocrystals under conditions where electron transfer can proceed to equilibrium was used to reveal which nanocrystals have more negative conduction-band potentials, and larger ($d \approx$ 4.0 nm) n-type $Zn_{0.75}Mg_{0.25}O$ nanocrystals were demonstrated to be better reductants than smaller ($d \approx$ 2.9 nm) n-type ZnO nanocrystals, despite less quantum confinement in the former. Finally, these data show that the visible trap luminescence can be used as a probe of the conduction-band potentials of $Zn_{1-x}Mg_xO$ nanocrystals at various diameters and values of x. Collectively, these results demonstrate that Mg^{2+} substitution is valuable for tuning the physical and chemical properties of colloidal ZnO-

dx.doi.org/10.1021/ja3019934 | J. Am. Chem. Soc. 2012, 134, 7937−7943

based semiconductor nanocrystals, broadening the range of chemical properties accessible with these unusual colloidal reductants. Future studies of these colloidal *n*-type nanocrystals as chemical reductants can be expected to yield important fundamental insights into both inter-nanocrystal and nanocrystal-molecule spontaneous electron transfer reactions relevant to a broad variety of catalytic and energy conversion technologies.

AUTHOR INFORMATION

Corresponding Author

gamelin@chem.washington.edu

Present Address

[†]Department of Chemistry, University of Massachusetts, Amherst, MA 01003

Notes

The authors declare no competing financial interest.

ACKNOWLEDGMENTS

This research was funded by the U.S. National Science Foundation (CHE 0628252-CRC and CHE 1151726).

REFERENCES

(1) Haase, M.; Weller, H.; Henglein, A. *J. Phys. Chem.* **1988**, *92*, 482−487.

(2) Shim, M.; Guyot-Sionnest, P. *J. Am. Chem. Soc.* **2001**, *123*, 11651−11654.

(3) Liu, W. K.; Whitaker, K. M.; Kittilstved, K. R.; Gamelin, D. R. *J. Am. Chem. Soc.* **2006**, *128*, 3910−3911.

(4) Liu, W. K.; Whitaker, K. M.; Smith, A. L.; Kittilstved, K. R.; Robinson, B. H.; Gamelin, D. R. *Phys. Rev. Lett.* **2007**, *98*, 186804.

(5) Whitaker, K. M.; Ochsenbein, S. T.; Polinger, V. Z.; Gamelin, D. R. *J. Phys. Chem. C* **2008**, *112*, 14331−14335.

(6) Whitaker, K. M.; Ochsenbein, S. T.; Smith, A. L.; Echodu, D. C.; Robinson, B. H.; Gamelin, D. R. *J. Phys. Chem. C* **2010**, *114*, 14467−14472.

(7) Hayoun, R.; Whitaker, K. M.; Gamelin, D. R.; Mayer, J. M. *J. Am. Chem. Soc.* **2011**, *133*, 4228−4231.

(8) van Dijken, A.; Mulenkamp, E. A.; Vanmaekelbergh, D.; Meijerink, A. *J. Phys. Chem. B* **2000**, *104*, 4355.

(9) Wood, A.; Giersig, M.; Mulvaney, P. *J. Phys. Chem. B* **2001**, *105*, 8810−8815.

(10) Subramanian, V.; Wolf, E. E.; Kamat, P. V. *J. Phys. Chem. B* **2003**, *107*, 7479−7485.

(11) Germeau, A.; Roest, A. L.; Vanmaekelbergh, D.; Allan, G.; Delerue, C.; Meulenkamp, E. A. *Phys. Rev. Lett.* **2003**, *90*, 097401.

(12) Hoyer, P.; Weller, H. *J. Phys. Chem.* **1995**, *99*, 14096−14100.

(13) Mohamed, H. H.; Mendive, C. B.; Dillert, R.; Bahnemann, D. W. *J. Phys. Chem. A* **2011**, *115*, 2139.

(14) Johnson, C. A.; Cohn, A.; Kaspar, T. C.; Chambers, S. A.; Salley, G. M.; Gamelin, D. R. *Phys. Rev. B* **2011**, *84*, 125203.

(15) Johnson, C. A.; Kittilstved, K. R.; Kaspar, T. C.; Droubay, T. C.; Chambers, S. A.; Salley, G. M.; Gamelin, D. R. *Phys. Rev. B* **2010**, *82*, 115202.

(16) Zippel, J.; Heitsch, S.; Stölzel, M.; Müller, A.; von Wenckstern, H.; Benndorf, G.; Lorenz, M.; Hochmuth, H.; Grundmann, M. *J. Lumin.* **2010**, *130*, 520.

(17) Gruber, T.; Krichner, C.; Kling, R.; Reuss, F.; Waag, A. *Appl. Phys. Lett.* **2004**, *84*, 5359.

(18) Lange, M.; Dietrich, C. P.; Zuniga-Perez, J.; von Wenckstern, H.; Lorenz, M.; Grundmann, M. *J. Vac. Sci. Technol. A* **2011**, *29*, 03A104.

(19) Park, W. I.; Yi, G.-C.; Kim, M. Y.; Pennycook, S. J. *Adv. Mater.* **2003**, *15*, 526.

(20) Gimenez, A. J.; Yáñez-Limón, J. M.; Seminario, J. M. *J. Phys. Chem. C* **2011**, *115*, 282−287.

(21) Zu, P.; Tang, Z. K.; Wong, G. K. L.; Kawasaki, M.; Ohtomo, A.; Koinuma, H.; Segawa, Y. *Solid State Commun.* **1997**, *103*, 459.

(22) Ohtomo, A.; Kawasaki, M.; Koida, T.; Masubuchi, K.; Koinuma, H.; Sakurai, Y.; Yoshida, Y.; Yasuda, T.; Segawa, Y. *Appl. Phys. Lett.* **1998**, *72*, 2466.

(23) Chiou, J. W.; Tsai, H. M.; Pao, C. W.; Krishna Kumar, K. P.; Ray, S. C.; Chien, F. Z.; Pong, W. F.; Tsai, M.-H.; Chen, C.-H.; Lin, H.-J.; Wu, J. J.; Yang, M.-H.; Liu, S. C.; Chiang, H. H.; Chen, C. W. *Appl. Phys. Lett.* **2006**, *89*, 043121.

(24) Su, S. C.; Lu, Y. M.; Zhang, Z. Z.; Shan, C. X.; Li, B. H.; Shen, D. Z.; Yao, B.; Zhang, J. Y.; Zhao, D. X.; Fan, X. W. *Appl. Phys. Lett.* **2008**, *93*, 082108.

(25) Minemoto, T.; Negami, T.; Nishiwaki, S.; Takakura, H.; Hamakawa, Y. *Thin Solid Films* **2000**, *372*, 173.

(26) Ding, R.; Xu, C.; Gu, B.; Shi, Z.; Wang, H.; Ba, L.; Xiao, Z. *J. Mater. Sci. Tech.* **2010**, *26*, 601.

(27) Wang, Y. S.; Thomas, P. J.; O'Brien, P. *J. Phys. Chem. B* **2006**, *110*, 21412.

(28) Yang, Y.; Jin, Y.; He, H.; Wang, Q.; Tu, Y.; Lu, H.; Ye, Z. *J. Am. Chem. Soc.* **2010**, *132*, 13381−13394.

(29) Shannon, R. D. *Acta Crystallogr. Sect. A: Foundations* **1976**, *32*, 751−767.

(30) Heitsch, S.; Zimmermann, G.; Fritsch, D.; Sturm, C.; Schmidt-Grund, R.; Schulz, C.; Hochmuth, H.; Spermann, D.; Benndorf, G.; Rheinländer, B.; Nobis, T.; Lorenz, M.; Grundmann, M. *J. Appl. Phys.* **2007**, *101*, 083521.

(31) Shan, F. K.; Kim, B. I.; Liu, G. X.; Liu, Z. F.; Sohn, J. Y.; Lee, W. J.; Shin, B. C.; Yu, Y. S. *J. Appl. Phys.* **2004**, *95*, 4772.

(32) Schwartz, D. A.; Norberg, N. S.; Nguyen, Q. P.; Parker, J. M.; Gamelin, D. R. *J. Am. Chem. Soc.* **2003**, *125*, 13205−13281.

(33) Norberg, N. S.; Kittilstved, K. R.; Amonette, J. E.; Kukkadapu, R. K.; Schwartz, D. A.; Gamelin, D. R. *J. Am. Chem. Soc.* **2004**, *126*, 9387−9398.

(34) West, A. R. *Solid State Chemistry and Its Applications*; John Wiley and Sons: New York, 1992.

(35) Meulenkamp, E. A. *J. Phys. Chem. B* **1998**, *102*, 5566−5572.

(36) Wood, A.; Giersig, M.; Hilgendorff, M.; Vilas-Campos, A.; Liz-Marzán, L. M.; Mulvaney, P. *Aust. J. Chem.* **2003**, *56*, 1051−1057.

(37) Norberg, N. S.; Gamelin, D. R. *J. Phys. Chem. B* **2005**, *109*, 20810−20816.

(38) Olson, D. C.; Shaheen, S. E.; White, M. S.; Mitchell, W. J.; van Hest, M. F. A. M.; Collins, R. T.; Ginley, D. S. *Adv. Funct. Mater.* **2007**, *17*, 264.

(39) Vanheusden, K.; Warren, W. L.; Seager, C. H.; Tallant, D. R.; Voigt, J. A.; Gnade, B. E. *J. Appl. Phys.* **1996**, *79*, 7983−7990.

(40) Leiter, F. H.; Alves, H. R.; Hofstaetter, A.; Hofmann, D. M.; Meyer, B. K. *Phys. Stat. Sol. b* **2001**, *226*, R4−R5.

(41) van Dijken, A.; Meulenkamp, E. A.; Vanmaekelbergh, D.; Meijerink, A. *J. Lumin.* **2000**, *90*, 123−128.

(42) van Dijken, A.; Makkinje, J.; Meijerink, A. *J. Lumin.* **2001**, *92*, 323−328.

(43) Hsu, N. E.; Hun, W. K.; Chen, Y. F. *J. Appl. Phys.* **2004**, *96*, 4671.

(44) Matsumoto, T.; Kato, H.; Miyamoto, K.; Sano, M.; Zhukov, E. A.; Yao, T. *Appl. Phys. Lett.* **2002**, *81*, 1231−1233.

(45) Zhou, H.; Alves, H.; Hofmann, D. M.; Kriegseis, W.; Meyer, B. K.; Kaczmarczyk, G.; Hoffmann, A. *Appl. Phys. Lett.* **2002**, *80*, 210−212.

(46) Bohle, D. S.; Spina, C. J. *J. Am. Chem. Soc.* **2007**, *129*, 12380−12381.

(47) Bohle, D. S.; Spina, C. J. *J. Am. Chem. Soc.* **2009**, *131*, 4397−4404.

(48) Qui, X.; Li, L.; Zheng, J.; Liu, J.; Sun, X.; Li, G. *J. Phys. Chem. C* **2008**, *112*, 12242.

(49) Zhang, X. D.; Guo, M. L.; Liu, C. L.; Zhang, L. A.; Zhang, W. Y.; Ding, Y. Q.; Wu, Q.; Feng, X. *Eur. Phys. J. B* **2008**, *62*, 417.

(50) Feng, Y.; Badaeva, E.; Gamelin, D. R.; Li, X. *J. Phys. Chem. Lett.* **2010**, *1*, 1927−1931.

(51) Badaeva, E.; May, J. W.; Ma, J.; Gamelin, D. R.; Li, X. *J. Phys. Chem. C* **2011**, *115*, 20986−20991.
(52) Dietl, T. *Phys. Rev. B* **2008**, *77*, 085208.
(53) Sokolov, V. I.; Druzhinin, A. V.; Gruzdev, N. B.; Dejneka, A.; Churpita, O.; Hubicka, Z.; Jastrabik, L.; Trepakov, V. *Phys. Rev. B* **2010**, *81*, 153104.
(54) Kittilstved, K. R.; Liu, W. K.; Gamelin, D. R. *Nat. Mater.* **2006**, *5*, 291−297.
(55) Norberg, N. S.; Dalpian, G. M.; Chelikowsky, J. R.; Gamelin, D. R. *Nano Lett.* **2006**, *6*, 2887−2892.
(56) Langer, J. M.; Delerue, C.; Lannoo, M.; Heinrich, H. *Phys. Rev. B* **1988**, *38*, 7723−7739.
(57) Caldas, M. J.; Fazzio, A.; Zunger, A. *Appl. Phys. Lett.* **1984**, *45*, 671−673.
(58) Orlinskii, S. B.; Schmidt, J.; Baranov, P. G.; Hofmann, D. M.; de Mello Donegá, C.; Meijerink, A. *Phys. Rev. Lett.* **2004**, *92*, 047603.
(59) Orlinskii, S. B.; Schmidt, J.; Groenen, E. J. J.; Baranov, P. G.; de Mello Donegá, C.; Meijerink, A. *Phys. Rev. Lett.* **2005**, *94*, 097602.
(60) Orlinskii, S. B.; Schmidt, J.; Baranov, P. G.; Lorrmann, V.; Riedel, I.; Rauh, D.; Dyakonov, V. *Phys. Rev. B* **2008**, *77*, 115334.
(61) Ochsenbein, S. T.; Feng, Y.; Whitaker, K. M.; Badaeva, E.; Liu, W. K.; Li, X.; Gamelin, D. R. *Nature Nanotechnol.* **2009**, *4*, 681−687.
(62) Wassner, T. A.; Laumer, B.; Althammer, M.; Goennenwein, S. T. B.; Stutzmann, M.; Eickhoff, M.; Brandt, M. S. *Appl. Phys. Lett.* **2010**, *97*, 092102.